

Article

Monitoring Damage in PC Slabs by Modal and Ultrasonic Tests

Sitthidon Kaewsawang^a, Wacharaphon Chaisiriniran^b, Poohrid Kaewngam^c,
and Piya Chotickai^{d,*}

Department of Civil Engineering, Kasetsart University, 50 Ngam Wong Wan Rd., Lat Yao, Chatuchak, Bangkok, 10900, Thailand

E-mail: ^asitthidon.ka@ku.th, ^bWacharaphon.ch@hotmail.com, ^cPoom.ce48@gmail.com,

^{d,*}fengpyc@ku.ac.th (Corresponding author)

Abstract. The effectiveness of modal and ultrasonic tests for monitoring the damage in precast prestressed concrete slabs was experimentally investigated. Four slabs with two different span lengths and corresponding modes of failure (interfacial shear and flexural failures) were subjected to loading steps until failure. The variations in fundamental natural frequency, damping ratio, ultrasonic pulse velocity (UPV), and ultrasonic wave attenuation in relation to the damage severity and failure mode were investigated and compared. It was observed that the natural frequency was sensitive to flexural crack development. A significant change in the damping ratio was obtained in the slabs with moderate damage. The UPV was not affected by a moderate degree of interfacial shear damage and a low degree of flexural damage; however, it was strongly related to the progression of flexural damage at the severe stage. Among the various indexes, ultrasonic wave attenuation was most sensitive to the development of damage. The method could detect interfacial-shear and flexural cracks at an early stage.

Keywords: Damage detection, damping, natural frequency, nondestructive test, prestressed concrete, ultrasonic, pulse velocity.

ENGINEERING JOURNAL Volume 27 Issue 2

Received 7 July 2022

Accepted 21 February 2023

Published 28 February 2023

Online at <https://engj.org/>

DOI:10.4186/ej.2023.27.2.17

1. Introduction

Precast prestressed concrete (PC) slabs are commonly used in building and bridge construction. They are used for making composite slabs with cast-in-place concrete topping, which improves the flexural and shear capacities of the slab and increases the floor diaphragm action [1]. An in-service prestressed slab can be damaged by overloading, material degradation, or accidental impact load. The prestressing force is applied to the full slab and may be great enough to close existing cracks when the slab is unloaded. This decreases the sensitivity of the structural dynamic and stress wave characteristics for damage detection [2, 3]. Therefore, damage monitoring is challenging, especially at the early stage of damage.

Various modal-based evaluation techniques have been used in other existing studies for monitoring the damage of concrete members [4-6]. These damage monitoring techniques employed variations in the structural dynamic characteristics, such as natural frequency, mode shape, and damping ratio, when subjected to forced, free, or ambient vibration. A modal test is a global damage evaluation technique, wherein the dynamic characteristics are determined from the global responses of members subjected to vibration. It is not sensitive to damage in members that have minute effects on the dynamic characteristics of the structures [7]. For uncracked PC beams, an increasing trend in fundamental natural frequency with the increase in prestressing force has been reported [8, 9]. Gharighoran et al. [4] investigated the shift in the natural frequencies of reinforced and post-tensioned concrete beams subjected to various degrees of damage. The prestressing force significantly decreased the change in the natural frequencies of the beams with respect to the increase in the degree of damage. Wang et al. [5] and Neild et al. [10] investigated the effect of damage degree on the nonlinear dynamic characteristics of reinforced concrete beams. The natural frequency gradually increased with an increase in the vibration displacement amplitude at a low degree of damage. However, the amplitude-dependent frequency behavior was observed to be insignificant for beams with moderate and severe degrees of damage.

The damping ratios of low-order fundamental modes (first to third modes) increase with the increase in damage severity in reinforced concrete members, which is caused by the friction between the crack surfaces and the formation of microcracks in the concrete [11]. The damping ratio is sensitive to the damage severity of the reinforced concrete members. However, the application of the parameter in damage identification is still limited because of the large scattering of results [12]. The difference in the damping ratios between undamaged and damaged PC members was reported to be marginal in some existing studies [13, 14].

Among various stress-wave-based nondestructive testing methods, ultrasonic testing has been widely used in some existing studies for detecting variations in the mechanical properties, cracks, and voids in concrete

materials [15-17]. Generally, it is recognized as a local damage evaluation technique that can identify damages only within the wave travel path. Several acoustic parameters, such as wave velocity, amplitude attenuation, and frequency shift, have been demonstrated to be potential damage indicators for concrete [18]. The ultrasonic pulse velocity (UPV) is one of the most commonly used parameters for evaluating severity of damages in concrete and has been standardized [19, 20]. This parameter is determined based on a linear ultrasonic test, whereas the overall shape of the ultrasonic wave is not affected as the wave propagates. For uncracked concrete, the UPV depends mainly on the density and elastic properties of the concrete [21]. For cracked concrete, the open cracks scatter and diffract stress waves, whereas the closed and partially closed cracks cause wave attenuation and increase the wave travel time [22]. This alters the wave characteristics and reduces the wave velocity and transmission amplitude in cracked concrete [23]. It has been shown in some of the existing studies [24, 25] that transmission amplitude and wave attenuation determined based on a nonlinear ultrasonic test, wherein the change in the shape of the propagating ultrasonic wave is considered, are sensitive to micro and macro defects in non-prestressed concrete.

When subjected to compressive stress, a portion of the stress wave is transmitted through the crack surfaces because of acoustic coupling, thereby increasing the wave velocity. The increase in magnitude is directionally dependent and sensitive to the compressive stress and roughness of the crack surfaces [26, 27]. Kee and Zhu [3] investigated the effects of external loadings on wave velocity and transmission amplitude across a flexural crack in reinforced concrete beams subjected to compressive force. The wave velocity and transmission amplitude were reported to increase with an increase in the applied force. The transmission amplitude was more sensitive to the change in crack width corresponding to an increase in the applied force than to wave velocity.

The present study focuses on the sensitivity of the indexes based on modal and ultrasonic tests for damage monitoring in PC slabs. The slabs with different span lengths were subjected to loading steps until failure. The effect of the increase in damage in the slabs on the variations in the linear dynamic characteristics (fundamental natural frequency and damping ratio) and linear and nonlinear ultrasonic wave characteristics (UPV and ultrasonic frequency spectrum) were investigated and compared.

2. Research Significance

Despite numerous attempts to monitor damage using modal and ultrasonic tests, the sensitivity of the test methods to detecting damage in PC slabs has not been thoroughly investigated. Additionally, most of the studies have been conducted concentrating on either one of the methods. Consequently, the variation in and relation of the evaluation results obtained from the methods is still

unclear. This paper presents a study on the effectiveness of the methods in monitoring the damage of PC slabs. The findings in this study will provide useful information on damage detection at an early stage and damage evaluation at various damage stages.

3. Experimental Procedure

The experimental program consisted of modal and ultrasonic tests of PC slabs subjected to loading steps under the four-point bending test. The modal and ultrasonic tests were conducted before subjecting the slabs to the bending test, referred to as the undamaged condition, and after each loading increase under the unloaded condition.

3.1. Specimen Description

Four PC slab specimens of 350 mm width and 100 mm thickness were prepared. The specimens for the four-point bending test consisted of two prestressed slabs of 2 m length and two slabs of 2.5 m length (denoted as S2.0 and S2.5), with span lengths of 1.8 m and 2.4 m, respectively. The specimens were prepared from 50-mm-thick precast PC slabs with 50-mm-thick cast-in-place concrete topping (see Fig. 1a).

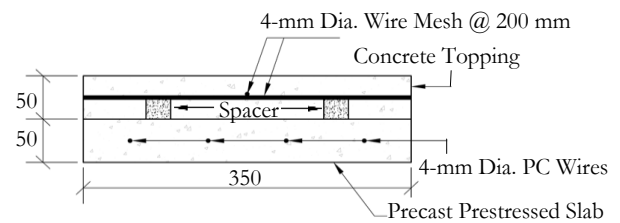
The precast and cast-in-place concrete were made from concrete with a maximum aggregate size of 19 mm and nominal compressive strengths of 35 MPa and 20.8 MPa, respectively. Each precast slab was prestressed with four 4 mm prestressing wires with the specified tensile strength and 0.1% offset yield strength of 1770 MPa and 1470 MPa, respectively. The jacking stress of the prestressing wires was equal to 94% of the yield strength, as specified in ACI 318-19 [28], and was used for prestressing the precast slabs. A wire mesh with 4 mm diameter and 200 mm spacing and specified tensile strength of 610 MPa was used to reinforce the cast-in-place concrete layer. The longitudinally broomed surface roughness of the precast slabs provided mechanical interlocking between the precast and cast-in-place concrete. The cast-in-place concrete was moist-cured for 28 days before being subjected to nondestructive and static bending tests.

3.2. Static Bending Test

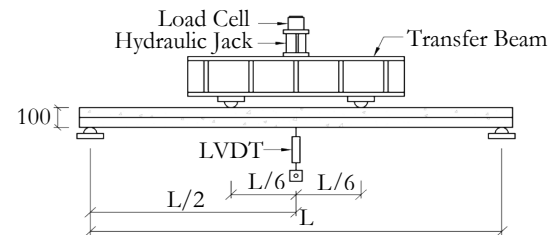
The specimens were subjected to a static load test under four-point bending with loading steps until failure. The force from the hydraulic jack was applied on the specimens through a transfer beam. The distances between the loading points on the S2.0 and S2.5 specimens were 600 and 800 mm, respectively. The applied load and mid-span vertical displacement were monitored by using a load cell and a linear variable displacement transducer (LVDT) (Fig. 1b). Four strain gauges (Fig. 1c) were affixed to the bottom and top surfaces. At the bottom surface, two strain gauges (SG nos. 1 and 2) were directly under the applied line loads

from the transfer beam, and a strain gauge (SG no. 3) was in the middle. A strain gauge (SG no. 4) was affixed on the top surface in the middle.

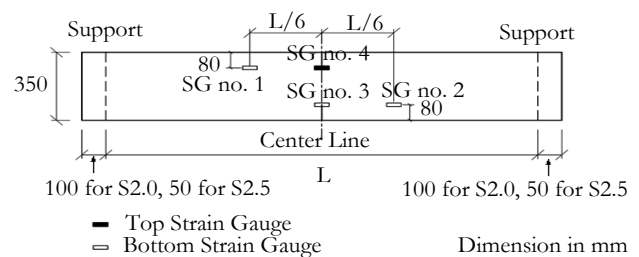
Incremental loading steps of approximately 2.45 and 1.96 kN were used for specimens S2.0 and S2.5, respectively. The higher load increment was employed for the S2.0 specimen to correspond to the higher flexural capacity estimated for the slabs with shorter span lengths. After each loading step, the hydraulic jack and transfer beam were removed, thereby leaving the slab unloaded before the modal and ultrasonic tests.



a) Cross section of the prestressed concrete slab



b) Test setup and LVDT measurement



c) Strain gauge monitoring

Fig. 1. Slab cross section and experimental setup.

3.3. Modal Test

The modal test was conducted on the specimens under unloaded conditions. Free vibration responses corresponding to the fundamental natural frequency of the specimens were generated by impacting with a 7.2 N rubber hammer at the middle. Six Tokyo Sokki ARF-50A one-directional acceleration transducers were used to measure vertical accelerations, as shown in Fig. 2a. A drop height of 150 mm was adopted for the test, thereby causing peak acceleration in the range 0.4–0.5g at the

middle. Three repetitive tests were conducted before and after each loading step, with a data sampling frequency of 200 Hz. The two modal-based indexes, natural frequency and damping ratio, were determined from the acceleration responses. The acceleration at each monitored location was transformed to the frequency domain using the fast Fourier transform (FFT) technique. The fundamental natural frequency was determined from the frequency with the highest amplitude in the frequency domain. Additionally, the damping ratio was obtained from the free vibration response of each accelerometer. At each loading step, the average values of the fundamental natural frequency and damping ratio were determined from all the accelerometers on the specimens.

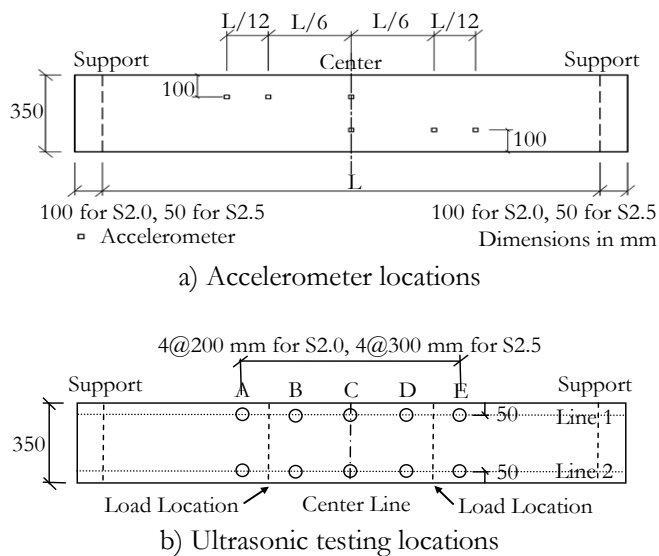


Fig. 2. Monitored locations of the modal and ultrasonic tests.

3.4. Ultrasonic Test

The ultrasonic test was conducted using a commercial ultrasonic testing instrument (Proceq Pundit Lab) with a nominal transducer frequency of 54 kHz. The UPV measurements were conducted using direct and indirect transmission. The measurements were based on the P-wave velocity. The transducers were placed opposite each other for direct transmission and were attached on the bottom surface for indirect transmission. For direct transmission, a transmitting transducer was placed opposite to the receiving transducer at 10 locations on five transverse locations (A to E) (Fig. 2b). The transverse locations A and E were located outside the constant moment region. The other transverse locations were located between the loading points of the transfer beam. During measurements, the transmitting transducer was fixed, while the receiving transducer was completely removed and reattached to obtain three readings. The signal was sampled with a sampling frequency of 2000 kHz, which was high enough to capture variation in ultrasonic waveforms. The waveforms were recorded and used for further analysis.

For indirect transmission, the transmitting and receiving transducers were placed between two

consecutive locations (between 1A and 1B, between 2A and 2B, and so on). Measurements were conducted at eight locations. Similar to direct transmission, three tests were repeated to obtain the pulse velocities and waveforms at each measurement location.

4. Experimental Results and Discussion

4.1. Load–Displacement Relationship

The results obtained from the bending tests are shown in Table 1. Specimens S2.0-1 and S2.0-2 withstood the ultimate loads of 7.29 kN and 7.41 kN, respectively, at the third loading step before failure. The failure was caused by delamination between the precast and cast-in-place concrete (Fig. 3a) in the fourth loading step, thereby resulting in premature failure. The failure loads were significantly lower than those of S2.5-1 and S2.5-2, which failed at the sixth loading step at the average ultimate load of 11.16 kN. These two specimens failed in the flexure mode (Fig. 3b).

The effects of load increase on the load-displacement relationship are shown in Fig. 4. At a low load level, the specimens exhibited a linear load-displacement relationship, wherein the flexural stress at the bottom surface was still in compression. As the applied load increased, the load-displacement relationship became nonlinear. Depending on the failure modes, the nonlinear behavior corresponded to crack opening, crack formation, and slippage at the interface. The nonlinear behavior was observed at several loading steps before the final step, thereby indicating that damage occurred at load levels significantly lower than the ultimate loads.

Table 1. Experimental results.

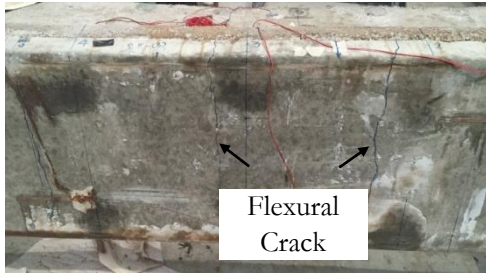
Specimen	P_{ult} (kN)	Properties of Undamaged Specimens				Failure Mode*
		UPV		Natural Freq. (Hz)	ζ (%)	
		DT (m/s)	IT (m/s)			
S2.0-1	7.29	3987	4576	35.6	2.42	SF
S2.0-2	7.41	3635	4563	41.3	1.40	SF
S2.5-1	11.77	4282	4511	28.6	0.99	FF**
S2.5-2	10.55	4012	4428	28.3	1.33	FF**

* SF = Shear failure at the interface between precast and cast-in-place concretes, FF = Flexural failure.

** Visible flexural cracks were developed in specimens S2.5-1 and S2.5-2 at 50.4% and 56.9% of the ultimate load, respectively.

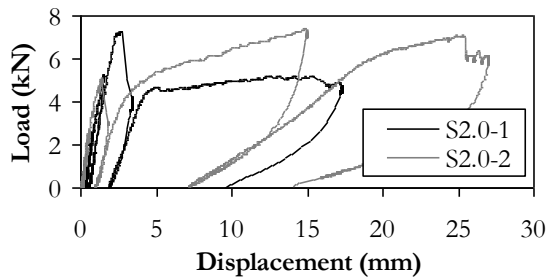


a) Interfacial shear failure

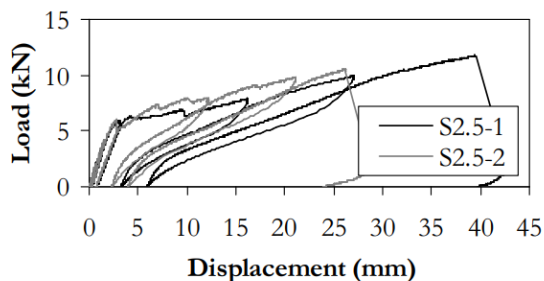


b) Flexural failure

Fig. 3. Failure mode of specimens.



a) Specimens S2.0



b) Specimens S2.5

Fig. 4. Load-displacement relationship.

The effect of the load increase on the initial stiffness is shown in Fig. 5. The stiffness ratio is the ratio of the stiffness of a particular loading step to that of the first loading step, whereas the degree of damage is represented by the ratio of the maximum load in the particular loading step to the specimen's ultimate load. Specimen S2.0-1 with interfacial shear failure exhibited a 13.0% reduction in the initial stiffness of the load-displacement relationship at a degree of damage of 71.8%. No significant reduction in the initial stiffness was observed in specimen S2.0-2 prior to the ultimate load. The S2.5-1 and S2.5-2 specimens with flexural failure exhibited 11.06–15.3% reductions in the initial stiffness at a degree of damage in the 50.4–56.9% range when the first visible flexural crack was observed.

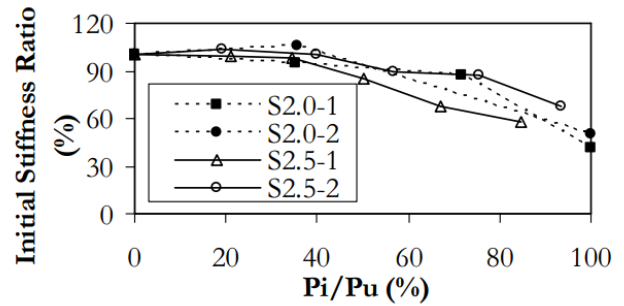


Fig. 5. Effect of load increase on the initial stiffness of the load-displacement relationship.

4.2. Effective Prestressing Stress

The effective prestressing stress was estimated from the relationship between the applied load and strain gauge data at the loading step after visible flexural cracks had developed at the gauge locations. Figure 6 shows the typical relationship between the load and strain gauge data of specimen S2.5-1 at applied loads of 50.4% and 66.9% of the ultimate load. Flexural cracks occurred when subjected to applied loads from the transfer beam and passed through strain gauge nos. 1 and 2 in the specimen. This plot shows a significant increase in the strain at 50.4% of the ultimate load, corresponding to the development of visible flexural cracks. At 66.9% of the ultimate load, the plot shows a bilinear response. Initially, a linear relationship was obtained. An increase in the applied load was accompanied by a proportional increase in the tensile strain. The tensile flexural strain was less than the prestressing compressive strain at this stage. At the second stage, the tensile flexural strain was higher than the prestressing compressive strain, thereby resulting in crack opening at the gauge location and a notable increase in the strain magnitude. The load corresponding to the end of the linear stage was used to estimate the effective prestressing force in the specimens. Based on the results obtained from the strain data of the S2.5-1 and S2.5-2 specimens, the applied loads at the crack opening were in the 4.82–5.34 kN range, corresponding to the effective prestressing force in the 54.1–58.7 kN range. Under unloaded conditions, the compressive stress at the flexural crack location ranged from 3.31 MPa–3.66 MPa.

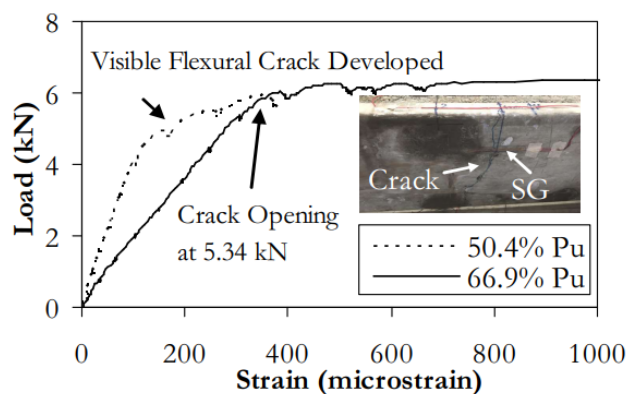
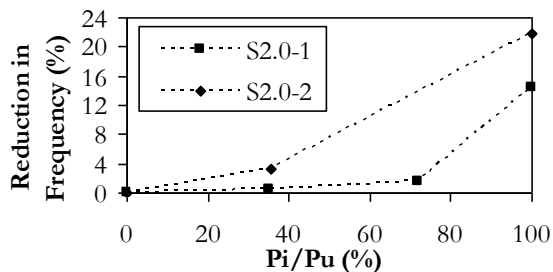


Fig. 6. Relationship between load and strain gauge no. 1 for specimen S2.5-1.

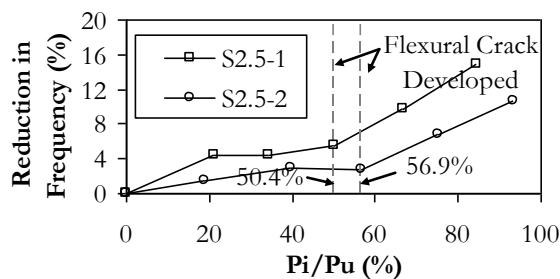
4.3. Fundamental Natural Frequency

The average values of the fundamental natural frequency of the undamaged specimens are shown in Table 1. The natural frequencies of the undamaged specimens with similar configurations were relatively close. The maximum COVs for different monitored locations were 0.24% and 2.97% for undamaged specimens and all loading steps, respectively. The COVs obtained from different locations increased marginally in the damaged specimens. The results indicated that changes in monitor locations had a minute effect on the natural frequency. This provided flexibility for the monitor locations. The parameters could be reliably determined without knowledge of the damage location.

The relationships between the percentage of reduction in the natural frequency and degree of damage are shown in Fig. 7. The natural frequency gradually decreased with the increase in damage at the low-damage level. When flexural cracks appeared, the reductions in the natural frequency were 5.55% and 2.74% for specimens S2.5-1 and S2.5-2, respectively. The natural frequencies significantly decreased after cracks appeared. For specimens with interfacial shear failure, the natural frequency decreased in the ranges of 0.40–3.17% and 1.43% at approximately 35% and 72% degrees of damage, respectively. No significant reduction in the natural frequency was observed before severe shear damage developed in the specimens.



a) Interfacial shear failure



b) Flexural failure

Fig. 7. Effects of the degree of damage on the fundamental natural frequency.

4.4. Damping Ratio

For the undamaged condition, the averages of the damping ratio (ζ) obtained from different monitored locations were in the ranges of 1.40–2.42% and 0.99–1.33% for specimens S2.0 and S2.5, respectively. The

damping ratio of specimen S2.0 with a higher fundamental natural frequency, corresponding to a shorter span length, was greater than that of specimen S2.5. In comparison with the natural frequency, a greater variation in the damping ratios among the specimens and monitored locations was observed. The maximum COVs for different monitored locations were 5.92% for the undamaged condition and increased to 10.3% for all loading steps.

The percentages of increase in the damping ratio at the particular loading step from that of the undamaged specimen are compared with the degrees of damage in Fig. 8. As the degree of damage increased, the damping ratio increased significantly, and large scattering among the specimens for degrees of damage higher than approximately 40% was observed. At this damage level, the percentages of change in the damping ratios were in the range of 10.9–35.7%. The results indicated that the damping ratio was more sensitive to change in damage than natural frequency, especially at the moderate stage of damage. No influence of the failure modes on the relationship between the increase in damping ratio and the degree of damage was observed.

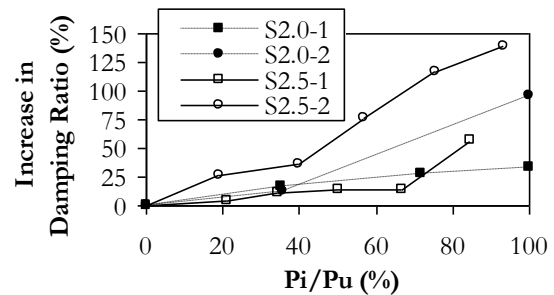


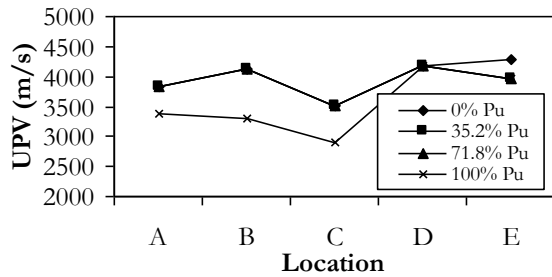
Fig. 8. Effects of the degree of damage on the damping ratio.

4.5. UPV

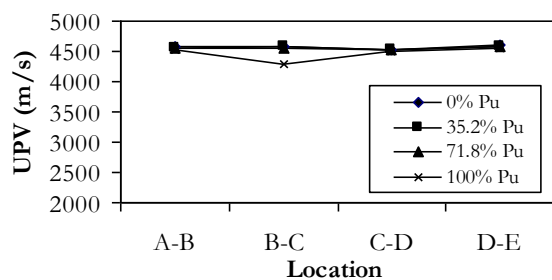
The average UPVs in the undamaged specimens are shown in Table 1. The direct and indirect transmission measurements are denoted by DT and IT, respectively. The COVs of the UPVs obtained from the different monitored locations in the specimens were in the ranges of 3.33–7.80% and 0.28–1.51% for the direct and indirect transmission, respectively. The higher average values and lower COVs of the UPVs obtained from indirect transmission than those of direct transmission indicated greater compressive strength and more homogeneous material properties of the near surface concrete (precast concrete) than those of the cast-in-place concrete.

Figure 9 shows a typical variation in the UPV with the increase in the degree of damage. The average UPVs obtained from direct and indirect transmission measurements at various transverse locations of specimens S2.0-1 with interfacial shear failure and S2.5-1 with flexural failure are shown. The crack formation in the concrete between the transmitting and receiving transducers resulted in the reduction in the UPV. A significant reduction in the UPV was observed in direct

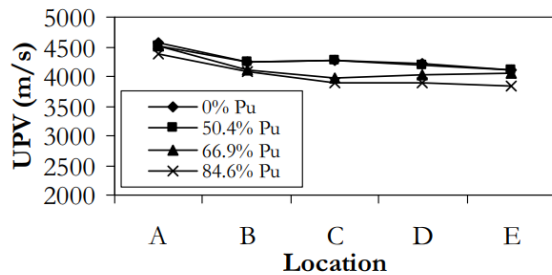
transmission, corresponding to interfacial shear failure in specimen S2.0-1. Such a reduction was not observed from indirect transmission in the specimen. A significant reduction in the UPVs from direct transmission indicated that interfacial shear cracks occurred at locations A, B, and C in the specimen.



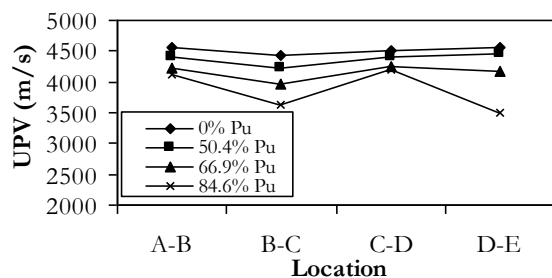
a) Direct transmission of S2.0-1



b) Indirect transmission of S2.0-1



c) Direct transmission of S2.5-1



d) Indirect transmission of S2.5-1

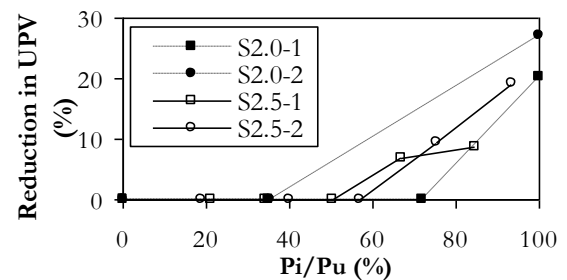
Fig. 9. UPVs along the specimen length at different degrees of damage.

In specimen S2.5-1, a reduction in the wave velocity of indirect transmission was observed at the degree of damage of 50.4% after the appearance of flexural cracks. At a lower degree of damage, no significant change in the UPV was observed. The prestressing compressive force was expected to hinder damage detection. For all load levels, the changes in the UPV from direct transmission were less than those from indirect transmission. This

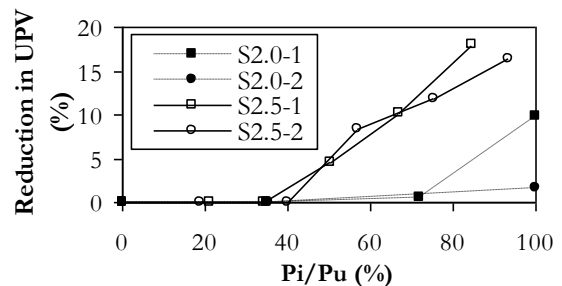
indicated the sensitivity of the measurement methods to the crack orientation. The indirect transmission method was more sensitive than the direct transmission method to flexural cracks.

To evaluate the sensitivity of the UPV to the damage in the specimens, the reductions in UPV at the location with the maximum change in the wave velocity were determined for each specimen and are shown in Fig. 10. For the S2.0-1 and S2.0-2 specimens with interfacial shear failure, significant reductions in the UPVs from direct and indirect transmissions were obtained at the ultimate load with a greater reduction percentage provided by the direct transmission. However, significant reductions in the UPVs were not observed at the loading step prior to the ultimate load.

For the S2.5-1 and S2.5-2 specimens with flexural failure, reductions in the wave velocity of 4.57% and 8.29% were obtained, respectively, at the development of visible flexural cracks corresponding to damage degrees of 50.4% and 56.9% in the specimens. The wave velocity decreased by 10.2–11.8% at 66.9–75.4% damage and decreased linearly with the increase in the degree of damage. The flexural cracks were in compression under the unloaded condition; however, the UPV provided an effective method of damage evaluation.



a) Direct transmission



b) Indirect transmission

Fig. 10. Variation in the UPV at different damage levels.

4.6. Ultrasonic Frequency Spectrum

To investigate the effect of the degree of damage on the variation in the frequency spectrum of ultrasonic waveforms, the waveforms in the time domain recorded at each location were transformed to the frequency domain using the FFT technique. Figure 11 shows the typical normalized spectra of ultrasonic waveforms. Frequencies around the central frequency of the transducer had relatively high amplitudes. A reduction in

the amplitudes, associated with wave attenuation, was obtained with an increase in the degree of damage.

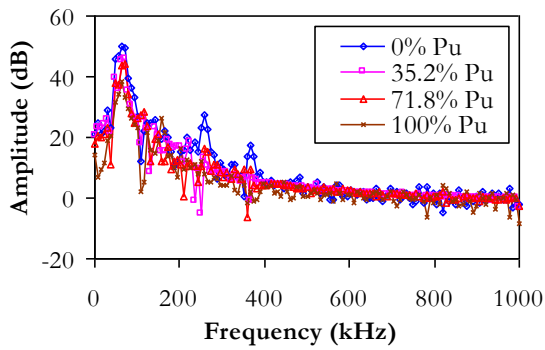
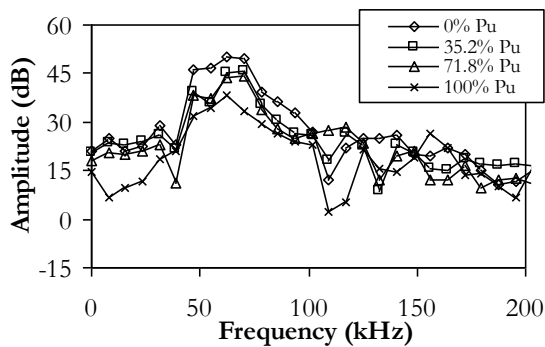
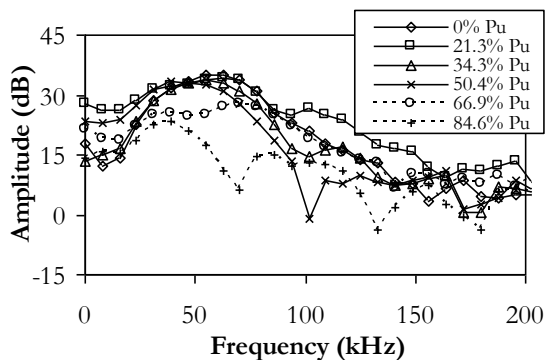


Fig. 11. Normalized spectra of ultrasonic waveforms from direct transmission of specimen S2.0-1.

Figure 12 shows the normalized spectra of ultrasonic waveforms of specimens S2.0-1 and S2.5-1 obtained from direct and indirect transmission methods, respectively. The variations in the fundamental frequency and frequency amplitude associated with wave attenuation with an increase in the degree of damage are shown in this figure. For the undamaged and low-damage stages, the fundamental frequency was 62.5 kHz, which was the central frequency of the transducer. The fundamental frequency decreased at the severe-damage stage (100% Pu) for specimens with interfacial shear failure and after visible flexural cracks developed (50.4% Pu for specimen S2.5-1) for specimens with flexural failure. The shift in the fundamental frequency was not affected by the interfacial and flexural cracks at the early stage of damage.



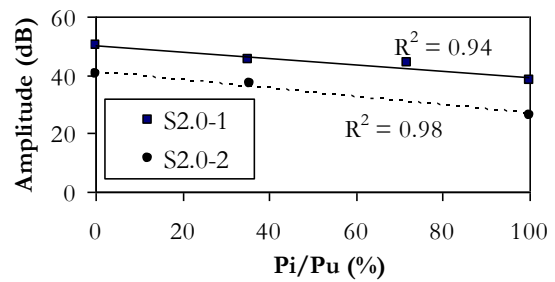
a) Direct transmission of specimen S2.0-1



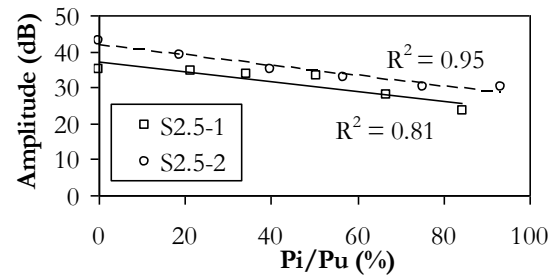
b) Indirect transmission of specimen S2.5-1

Fig. 12. Normalized spectra of ultrasonic waveforms.

The relationships between the ultrasonic frequency amplitude and the degree of damage are shown in Fig. 13. The maximum frequency amplitudes obtained from direct and indirect transmission methods are shown for the specimens that exhibited interfacial shear and flexural failures, respectively. This figure shows the linear relationship between the ultrasonic frequency amplitude and the degree of damage for both methods. Notwithstanding the low effectiveness of the UPV for damage identification at low degrees of damage, especially for specimens with interfacial shear failure, a decrease in the frequency amplitude, with a strong linear relation to the degree of damage, was observed in the specimens. This indicated the potential use of the frequency amplitude in damage detection and evaluation of the specimens with interfacial shear and flexural failures.



a) Direct transmission



b) Indirect transmission

Fig. 13. Effects of the degree of damage on ultrasonic frequency amplitude.

4.7. Comparison of Modal and Ultrasonic Tests

The comparisons of the degree of damage and the percentage of change in the modal- and ultrasonic-based indexes for interfacial shear and flexural failures are shown in Fig. 14. The percentages of reduction in the fundamental natural frequency, UPV, and ultrasonic frequency amplitude and the percentage of increase in the damping ratio are shown as the percentage of change in the figure. The percentage reductions in the UPV from direct and indirect transmission methods are compared with the degree of damage for interfacial shear and flexural failures, respectively. For clarity, the percentage of change in the damping ratio greater than 40% is not shown in the figure. For each index, a linear regression line was fitted to all data from the degree of damage, which the variation in the index started to obtain, to failure. The regression line was not fitted to the UPV for interfacial shear failure (Fig. 14a) because no significant reduction in the UPV was

obtained prior to the ultimate load for this failure mode. Table 2 shows the slope (a), intercept (c), coefficient of determination (R^2), and standard error of the estimate provided by the regression line. The standard error of the estimate (σ_{est}) was computed from

$$\sigma_{est} = \sqrt{\frac{\sum (Y - Y')^2}{N}} \quad (1)$$

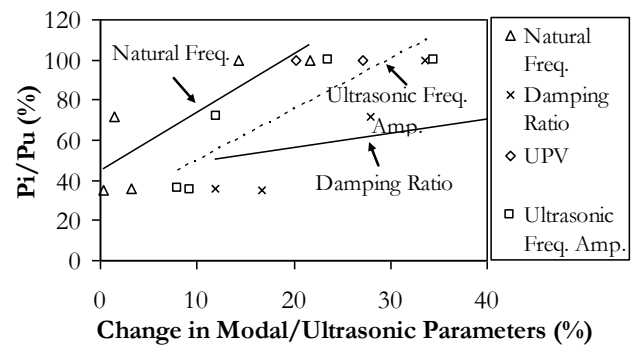
where Y and Y' are the actual and predicted degrees of damage, respectively, and N is the number of data points.

Table 2. Linear regression parameters of ultrasonic and modal test.

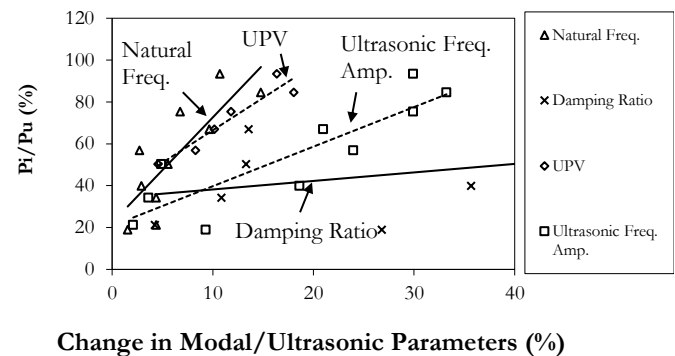
Parameter	Test Method	a	c	R^2	σ_{est}
Interfacial Shear Failure					
Natural Freq.	Modal	2.90	44.7	0.71	15.7
Damping Ratio	Modal	0.71	42.3	0.54	19.7
UPV	Ultrasonic	-	-	-	-
Ultrasonic Freq. Amp.	Ultrasonic	2.53	24.3	0.78	13.5
Flexural Failure					
Natural Freq.	Modal	5.03	22.3	0.66	14.2
Damping Ratio	Modal	0.41	34.1	0.55	16.4
UPV	Ultrasonic	3.10	35.5	0.90	4.65
Ultrasonic Freq. Amp.	Ultrasonic	1.89	20.8	0.75	12.2

The slopes and intercepts of the regression lines represented sensitivity to the progress of damage and the capability of damage detection at an early stage, respectively. The lower value of the slope indicated greater sensitivity to the progress of damage, while a lower value of the intercept indicated better capability of damage detection.

For modal-based indexes, a variation in the damping ratio was obtained in the specimens with moderate damage (42.3% and 34.1% of the ultimate loads for interfacial shear and flexural failures, respectively). The relative low values of R^2 were obtained for this parameter, corresponding to its large scattering at moderate and severe stages (Fig. 8). The damping ratio was capable of detecting interfacial shear cracks at a lower degree of damage compared to the capability of the fundamental natural frequency. Meanwhile, the fundamental natural frequency was more sensitive to the development of flexural cracks compared to the sensitivity of the damping ratio. After detecting damages, the fundamental natural frequency gradually changed with the increase in the degree of damage and provided a more accurate estimate of the degree of damage than that of the damping ratio, corresponding to its lower standard error of the estimate.



a) Shear failure at the interface between the precast and cast-in-place concrete



b) Flexural failure

Fig. 14. Comparison of modal- and ultrasonic-based indexes on damage monitoring.

Among the modal- and ultrasonic-based indexes, the UPV had the greatest value of the intercept for flexural failure. Additionally, it was incapable of detecting shear damage prior to failure. This indicated that the UPV was least sensitive of all the indexes in detecting damage. This parameter was capable of detecting moderate flexural damage (35.5% of the ultimate load). Consequently, the specimens were indicated to be damaged based on the modal indexes; however, the detailed inspection of the UPV might not be able to identify the damage. Furthermore, once the flexural damage were detected by the UPV, the change in the parameter had a strong linear relationship with the progress of damage and provided a relatively accurate estimate on the degree of damage, corresponding to its highest value of the coefficient of determination and lowest standard error of the estimate.

The ultrasonic frequency amplitude was most sensitive for damage detection, corresponding to its lowest value of the intercept. The changes in this parameter were obtained at the early stages of damage (24.3% and 20.8% of the ultimate loads for shear and flexural failures, respectively). The ultrasonic frequency amplitude had a lower slope of the linear regression line than that of the UPV for specimens with flexural failure. This indicated that for flexural cracks under compression, the ultrasonic frequency amplitude was more sensitive than the UPV to the progress of damage. Despite a strong linear relationship between the ultrasonic frequency amplitude and the degree of damage in each specimen (Fig. 13), a variation in the relationship among the specimens was

observed. For the degrees of damage that were not detected by the modal-based indexes, the regression parameters of the ultrasonic frequency amplitude, presented in Table 2, provided the maximum differences between the actual and predicted degrees of 12.6% and 3.5% for specimens with interfacial shear and flexural failures, respectively. The ultrasonic frequency amplitude provided a reasonable estimate of the degree of damage, especially at early and moderate degrees of damage.

5. Conclusions

Modal and ultrasonic tests were conducted to identify damage in prestressed concrete slabs subjected to loading steps under a four-point bending test. Several parameters, including the fundamental natural frequency, damping ratio, UPV, and ultrasonic frequency spectrum corresponding to different degrees of damage and failure modes, were investigated. The following conclusions can be drawn:

1. For the indexes based on the modal test, the fundamental natural frequency was sensitive to flexural crack development in the PC slabs. However, the parameter was insensitive to the development of interfacial shear cracks. The damping ratio was effectively demonstrated as a potential indicator for detecting the interfacial shear and flexural damages at the moderate stage.

2. Irrespective of a local damage evaluation technique, the UPV was less effective than the modal-based indexes in detecting damage, especially for interfacial shear cracks. However, this parameter provided a relatively accurate estimation of the degree of damage for specimens with moderate flexural damage.

3. Among the modal- and ultrasonic-based indexes, the ultrasonic frequency amplitude was most sensitive to damage development. This parameter could detect damage at an early stage before detection by the natural frequency and damping ratio. This parameter could be used to provide a reasonable estimation of the degree of damage at the early and moderate stages.

Acknowledgement

This study was financially supported by Kasetsart University Research and Development Institute (KURDI).

References

- [1] R. M. Mones and S. F. Breña, "Hollow-core slabs with cast-in-place concrete toppings: A study of interfacial shear strength," *PCI J*, vol. 58, no. 3, pp. 124-141, 2013.
- [2] M. P. Limongelli, D. Siegert, E. Merliot, J. Waeytens, F. Bourquin, R. Vidal, V. Le Corvec, I. Gueguen, and L. M. Cottineau, "Damage detection in a post tensioned concrete beam—Experimental investigation," *Eng Struct*, vol. 128, pp. 15-25, 2016.
- [3] S. H. Kee and J. Zhu, "Surface wave transmission across a partially closed surface-breaking crack in concrete," *ACI Mater J*, vol. 111, no. 1, pp. 35-46, 2014.
- [4] A. Gharighoran, F. Daneshjoo, and N. Khaji, "Use of Ritz method for damage detection of reinforced and post-tensioned concrete beams," *Constr Build Mater*, vol. 23, no. 9, pp. 2167-2176, 2009.
- [5] L. Wang, X. Zhou, H. Liu, and W. Yan, "Damage detection of RC beams based on experiment and analysis of nonlinear dynamic characteristics," *Constr Build Mater*, vol. 29, pp. 420-427, 2012.
- [6] M. U. Hanif, Z. Ibrahim, M. Jameel, K. Ghaedi, and M. Aslam, "A new approach to estimate damage in concrete beams using non-linearity," *Constr Build Mater*, vol. 124, pp. 1081-1089, 2016.
- [7] S. W. Doebling, C. R. Farrar, and M. B. Prime, "A summary review of vibration-based damage identification methods," *The Shock and Vibration Digest*, vol. 30, no. 2, pp. 91-105, 1998.
- [8] D. Noble, M. Nogal, A. O'Connor, and V. Pakrashi, "The effect of prestress force magnitude and eccentricity on the natural bending frequencies of uncracked prestressed concrete beams," *J Sound Vib*, vol. 365, pp. 22-44, 2016.
- [9] M. Saïidi, B. Douglas, and S. Feng, "Prestress force effect on vibration frequency of concrete bridges," *J Struct Eng*, vol. 120, no. 7, pp. 2233-2241, 1994.
- [10] S. A. Neild, M. S. Williams, and P. D. McFadden, "Nonlinear vibration characteristics of damaged concrete beams," *J Struct Eng*, vol. 129, no. 2, pp. 260-268, 2003.
- [11] Z. Nie, H. Hao, and H. Ma, "Structural damage detection based on the reconstructed phase space for reinforced concrete slab: experimental study," *J Sound Vib*, vol. 332, no. 4, pp. 1061-1078, 2013.
- [12] R. Perera, C. Huerta, and J. M. Orquín, "Identification of damage in RC beams using indexes based on local modal stiffness," *Constr Build Mater*, vol. 22, no. 8, pp. 1656-1667, 2008.
- [13] M. Kato and S. Shimada, "Vibration of PC bridge during failure process," *J Struct Eng*, vol. 112, no. 7, pp. 1692-1703, 1986.
- [14] M. G. Masciotta, L. F. Ramos, P. B. Lourenço, and M. Vasta, "Damage detection on the Z24 bridge by a spectral-based dynamic identification technique," *Proceedings of the 32nd IMAC, A Conference and Exposition on Structural Dynamics*, pp. 197-206, 2014.
- [15] C. W. In, R. B. Holland, J. Y. Kim, K. E. Kurtis, L. F. Kahn, and L.J. Jacobs, "Monitoring and evaluation of self-healing in concrete using diffuse ultrasound," *NDT & E Int*, vol. 57, pp. 36-44, 2013.
- [16] M. Benaïcha, O. Jalbaud, A. H. Alaoui, and Y. Burtschell, "Correlation between the mechanical behavior and the ultrasonic velocity of fiber-reinforced concrete," *Constr Build Mater*, vol. 101, no. 1, pp. 702-709, 2015.
- [17] E. Hwang, G. Kim, G. Choe, M. Yoon, N. Gucunski, and J. Nam, "Evaluation of concrete

- degradation depending on heating conditions by ultrasonic pulse velocity,” *Constr Build Mater*, vol. 171, pp. 511-520, 2018.
- [18] J. W. Ju, L. S. Weng, and Y. Liu, “Ultrasonic frequency-dependent amplitude attenuation characteristics technique for nondestructive evaluation of concrete,” *ACI Mater J*, vol. 103, no. 3, pp. 177-185, 2006.
- [19] *Standard Test Method for Pulse Velocity through Concrete*, ASTM C597-16, West Conshohocken, PA., 2016.
- [20] *Testing Concrete. Determination of Ultrasonic Pulse Velocity*, BS EN 12504-4:2004, 2004.
- [21] M. Hassan, O. Burdet, and R. Favre, “Ultrasonic measurements and static load tests in bridge evaluation,” *NDT & E Int*, vol. 28, no. 6, pp. 331-337, 1995.
- [22] L. Pahlavan, F. Zhang, G. Blacqui er, Y. Yang, and D. Hordijk, “Interaction of ultrasonic waves with partially-closed cracks in concrete structures,” *Constr Build Mater*, vol. 167, pp. 889-906, 2018.
- [23] W. Zhong and W. Yao, “Influence of damage degree on self-healing of concrete,” *Constr Build Mater*, vol. 22, no. 6, pp. 1137-1142, 2008.
- [24] A. A. Shah, Y. Ribakov, and Ch. Zhang, “Efficiency and sensitivity of linear and non-linear ultrasonics to identifying micro and macro-scale defects in concrete,” *Mater Des*, vol. 50, pp. 905-916, 2013.
- [25] C. M. Aldea, W. J. Song, J. S. Popovics, and S. P. Shah, “Extent of healing of cracked normal strength concrete,” *J Mater Civ Eng*, vol. 12, no. 1, pp. 92-96, 2000.
- [26] J. Y. Kim, A. Baltazar, and S. I. Rokhlin, “Ultrasonic assessment of rough surface contact between solids from elastoplastic loading-unloading hysteresis cycle,” *J Mech Phys Solids*, vol. 52, no. 8, pp. 1911-1934, 2004.
- [27] P. Shokouhi, A. Zo ga, H. Wiggenger, and G. Fischer, “Surface wave velocity-stress relationship in uniaxially loaded concrete,” *ACI Mater J*, vol. 109, no. 2, pp. 141-148, 2012.
- [28] ACI (American Concrete Institute), *Building Code Requirements for Structural Concrete and Commentary*, ACI 318-19, Farmington Hills, MI, USA, 2019.

Sitthinon Kaewsawang, photograph and biography not available at the time of publication.

Wacharaphon Chaisiriniran, photograph and biography not available at the time of publication.

Poohrid Kaewngam, photograph and biography not available at the time of publication.

Piya Chotickai, photograph and biography not available at the time of publication.